Research article

Xiaohan Cui, Kun Ding, Jian-Wen Dong and C.T. Chan*

Realization of complex conjugate media using non-PT-symmetric photonic crystals

https://doi.org/10.1515/nanoph-2019-0389
Received September 26, 2019; accepted November 14, 2019

Abstract: Although parity-time (PT)-symmetric systems can exhibit real spectra in the exact PT-symmetry regime, PT-symmetry is actually not a necessary condition for the real spectra. Here, we show that non-PT-symmetric photonic crystals (PCs) carrying Dirac-like cone dispersions can always exhibit real spectra as long as the average non-Hermiticity strength within the unit cell for the eigenstates is zero. By building a non-Hermitian Hamiltonian model, we find that the real spectra of the non-PT-symmetric system can be explained using the concept of pseudo-Hermiticity. We demonstrate using effective medium theories that, in the long-wavelength limit, such non-PT-symmetric PCs behave like the so-called complex conjugate medium (CCM) whose refractive index is real but whose permittivity and permeability are complex numbers. The real refractive index for this effective CCM is guaranteed by the real spectrum of the PCs, and the complex permittivity and permeability come from non-PT-symmetric loss-gain distributions. We show some interesting phenomena associated with CCM, such as the lasing effect.

Keywords: non-Hermitian photonic crystals; pseudo-Hermiticity; effective medium theory; laser.

***Corresponding author: C.T. Chan,** Department of Physics, The Hong Kong University of Science and Technology, Clear Water Bay, Kowloon, 999077 Hong Kong SAR, China, e-mail: phchan@ust.hk
Xiaohan Cui: Department of Physics, The Hong Kong University of Science and Technology, Clear Water Bay, Kowloon, 999077 Hong Kong SAR, China. https://orcid.org/0000-0003-2618-4509
Kun Ding: Department of Physics, The Hong Kong University of Science and Technology, Clear Water Bay, Kowloon, 999077 Hong Kong SAR, China; and The Blackett Laboratory, Department of Physics, Imperial College London, London SW7 2AZ, United Kingdom
Jian-Wen Dong: School of Physics and State Key Laboratory of Optoelectronic Materials and Technologies, Sun Yat-Sen University, Guangzhou 510275, China

1 Introduction

Hermitian Hamiltonian can describe ideal closed physical systems, in which the total energy is conserved and eigenfrequencies are purely real. However, nonconservative elements are ubiquitous in classical wave systems, and we need to introduce the concept of non-Hermiticity to describe such systems. In the past decades, there is a surge of interest in studying the physics of non-Hermitian systems [1–7] and the parity-time (PT)-symmetric system, which was first introduced in quantum mechanics [1], is the most popular one. A Hamiltonian H is said to be PT-symmetric if $[H, PT] = 0$, where the operator P represents a space reflection and the operator T represents a time reversal. PT-symmetric systems have been realized in optics and photonics [8–10]. In an optical system, the loss-gain (represented by the imaginary part of the refractive index) distribution is PT-symmetric if the complex-valued refractive index satisfies $n(x) = n^*(-x)$.

The most intriguing property of a PT-symmetric Hamiltonian is that it can exhibit real spectra in the exact PT-symmetry regime [2]. As we change the parameters of the Hamiltonian, such as the loss-gain strength, it may go into the broken PT-symmetry regime, and the eigenvalues form complex conjugate pairs. The symmetry-breaking point, marking the phase transition in the eigenvalue spectrum, is the exceptional point (EP) [11, 12]. However, PT-symmetry is not a necessary condition for achieving a real spectrum [13] and some studies about realizing real spectra in non-PT-symmetric systems have been presented recently [14–18]. It has been proven that the necessary condition for the real spectrum is pseudo-Hermiticity [13]. A Hamiltonian H satisfying $\eta H \eta^{-1} = H^\dagger$, where η is an invertible linear Hermitian operator, is defined as pseudo-Hermitian Hamiltonian (see Supplementary Note 1 for details). Real spectra realized in non-PT-symmetric systems can be explained using the concept of pseudo-Hermiticity.

Achieving the real spectra in a non-PT-symmetric photonic crystals (PC) is highly desirable as, from an effective medium (EM) theory (EMT) point of view [19], realizing the real spectra in certain regions of the Brillouin zone can lead to new applications. For example, one can then

realize a complex conjugate medium (CCM) [20–22], which carries many unusual phenomena, including coherent perfect absorption and lasing [23], and negative refraction [24]. The refractive index of CCM is a real number, but the permittivity and permeability can both be complex numbers in general [20]. From the EMT point of view, achieving a CCM using a PC requires the non-Hermitian PC to exhibit real frequency bands near the Brillouin zone center (Γ point) as the effective refractive index is real.

To understand the underlying physics, we build a two-band non-Hermitian Hamiltonian model for non-PT-symmetric PCs. We show that the model Hamiltonian is pseudo-Hermitian as long as the average non-Hermiticity strength (to be defined below) within the unit cell for the relevant states is zero and this condition can always be achieved in PCs that have Dirac-like cone dispersions. Consequently, real spectra can be realized in a particular frequency range, implying that the effective refractive index is real. In the long-wavelength limit, the scattering properties of such an inhomogeneous PC behave indeed like a homogeneous CCM.

2 Two-band non-Hermitian Hamiltonian model

As shown in Figure 1A (inset), we consider a two-dimensional (2D) PC with rods arranged in a square lattice in the $x-y$ plane. Within the unit cell with a lattice constant a, the rod (domain A, the blue region) having a radius r_c and relative permittivity $\varepsilon_A=\varepsilon_{cr}+i\gamma$ is embedded in a background medium (domain B, the gray region) with relative permittivity $\varepsilon_B=\varepsilon_{br}+i\ell_r\gamma$. We set $\varepsilon_{br}=1$ in the calculation and the relative permeability μ of both media as 1.0. The positive (negative) sign of γ indicates that the rod consists of a lossy (active) medium. A positive sign of ℓ_r indicates that the rod and background are either both lossy or both active, whereas a negative sign means that one is lossy and the other is active.

We study the PC in the transverse-magnetic polarization, where electric field $\mathbf{E}=E\hat{z}$ is normal to the $x-y$ plane, and electromagnetic waves propagate in the plane. As shown in Figure 1A, in the Hermitian limit ($\gamma=0$), this system has a Dirac-like cone dispersion [25] at the Brillouin zone center induced by accidental degeneracy. Compared to the Dirac cone of graphene system at the Brillouin zone corner, there is an additional flat band in the Dirac-like cone. It has been experimentally confirmed that the radiation existing in an open system can spawn rings of EPs in the wave vector space $\mathbf{k}=(k_x, k_y)$ out of Dirac-like

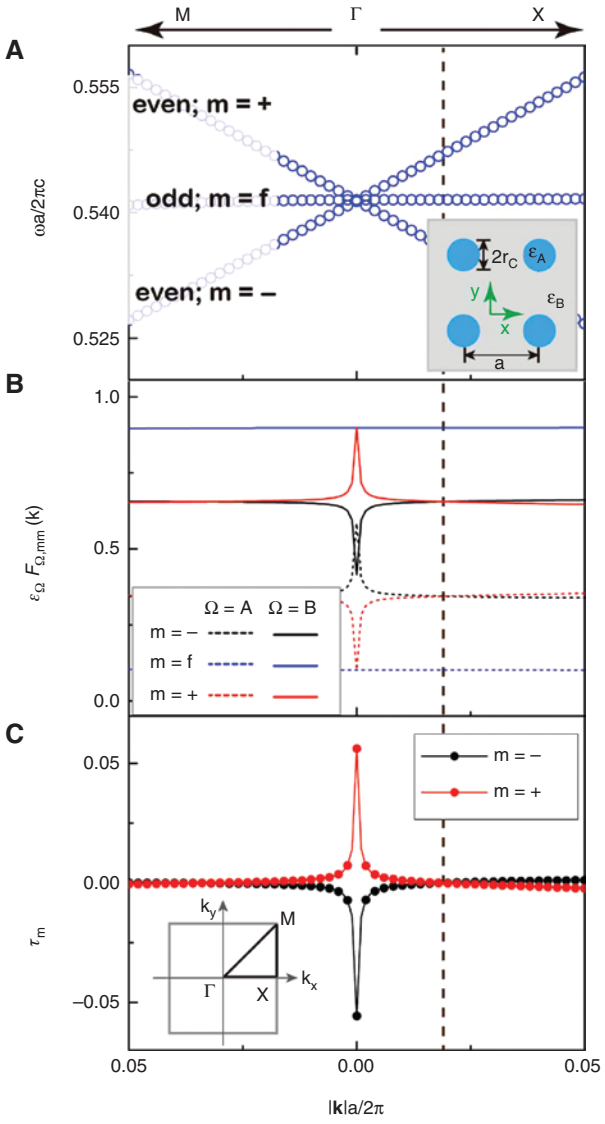

Figure 1: Properties of the Dirac-like cone.
(A) Band dispersions of Hermitian PC ($\gamma=0$) calculated using COMSOL. (B) Eigenmode profiles of top band $m=+$ (even mode), flat band $m=f$ (odd mode), and bottom band $m=-$ (even mode). (C) Average non-Hermiticity τ_m when gain-to-loss ratio $\ell_r=-0.15235$. The vertical dashed line denotes the intersection: $F_{\Omega,++}=F_{\Omega,--}$. (A, inset) Schematic of 2D PC constructed with cylinders (the blue areas); the gray area denotes air. (C, inset) First Brillouin zone of the square lattice. The parameters used are $r_c=0.1999a$, $\varepsilon_A=12.5+i\gamma$, and $\varepsilon_B=1+i\gamma\ell_r$.

cones [26], but imaginary parts of the eigenfrequencies are negative because of radiation loss. Now, we will see whether we can tune the bands outside the ring to become real spectra by adding gain into the system. In principle, the eigenfrequency and eigenfunction of Bloch states for this non-Hermitian 2D PC can be obtained by numerically solving the Helmholtz equation [27]. However, to study the

band structure of the non-Hermitian PC analytically, we construct a model Hamiltonian using Hermitian system's Bloch states obtained at a fixed value of $\mathbf{k}$ as the bases and obtain a generalized eigenvalue problem as (see Supplementary Note 3 for details) [28].

$$H_2 p_{\mathbf{k}n} = (\omega_{\mathbf{k}n}/c)^2 H_1 \cdot p_{\mathbf{k}n}, \tag{1}$$

where c is the speed of light and $\omega_{\mathbf{k}n}$ and $p_{\mathbf{k}n}$ are the eigenfrequencies and eigenvectors of the non-Hermitian system ($\gamma \neq 0$), respectively. The matrices in Equation (1) are $(H_1)_{mm'} = \delta_{mm'} + i\gamma(F_{A,mm'} + \ell_r F_{B,mm'})$ and $(H_2)_{mm'} = \delta_{mm'}(\omega_{km}^{(0)}/c)^2$. $\omega_{km}^{(0)}$ is the eigenfrequency of the Hermitian PC. To characterize the eigenmode profiles, we introduce a quantity

$$F_{\Omega,mm'} = \int_{\Omega} \mathrm{d}^2 r u_{\mathbf{k}m'}^{(0)*}(\mathbf{r}) u_{\mathbf{k}m}^{(0)}(\mathbf{r}), \tag{2}$$

where Ω denotes the rod ($|\mathbf{r}| < r_c$) or air ($|\mathbf{r}| > r_c$) domain. $F_{\Omega,mm'}$ ($m \neq m'$) expresses the overlapping between two different eigenmodes in the domain Ω, and $F_{\Omega,mm}$ expresses the amplitude distribution of the eigenmode m in the domain Ω. $u_{\mathbf{k}m}^{(0)}(\mathbf{r})$ is the eigenvector of the Hermitian PC ($\gamma = 0$) and satisfies the orthonormal relation

$$\varepsilon_A F_{A,mm'} + \varepsilon_B F_{B,mm'} = \delta_{mm'}, \tag{3}$$

where $\varepsilon_A = \varepsilon_{cr}$ denotes the relative permittivity of the rod domain and $\varepsilon_B = \varepsilon_{br} = 1$ represents the relative permittivity of the air domain. For convenience, we can omit the subscript $\mathbf{k}$ for simplicity and rewrite Equation (1) as $H \cdot p_n = W_n p_n$, where $W_n = (\omega_n/c)^2$ and $H = H_1^{-1} \cdot H_2$.

From Equation (2), we know that the function $F_{\Omega,mm'}$ involves the spatial integrations of eigenfunctions of Hermitian systems; hence, the symmetry of the eigenmode profile plays an important role here. In our system, we choose the center of the rod as origin. The even/odd symmetry characters are labeled in Figure 1A [27, 29]. As the two linearly dispersive bands ($m = \pm$) are even, whereas the flat band ($m = f$) is an odd mode, the matrix elements $F_{\Omega,+f}$ and $F_{\Omega,-f}$ are all zero, implying that there is no coupling between the flat band and the linear bands. Therefore, we can decouple the flat band from the Hamiltonian model and write the Hamiltonian as a 2×2 matrix (see Supplementary Note 3 for details):

$$H = \frac{1}{\beta}\begin{pmatrix} W_-^{(0)}(1 + i\gamma\tau_-) & -i\gamma\kappa W_+^{(0)} \\ -i\gamma\kappa^* W_-^{(0)} & W_+^{(0)}(1 + i\gamma\tau_+) \end{pmatrix}, \tag{4}$$

where $\beta = 1 + i\gamma(\tau_- + \tau_+) + \gamma^2(|\kappa|^2 - \tau_-\tau_+)$. In Equation (4),

$$\tau_m = F_{A,mm} + \ell_r F_{B,mm}, \quad (m = \pm) \tag{5}$$

is a real number, representing the average non-Hermiticity of state m within the primitive unit cell, and

$$\kappa = F_{A,-+} + \ell_r F_{B,+-}, \tag{6}$$

is a complex number, representing an overlapping between the two eigenmodes. According to Equation (5), the values of $\tau_\pm$ depend not only on the distributions of non-Hermiticity (described by ℓ_r) in the unit cell but also on the eigenmode profiles (as described by $F_{\Omega,mm}$). The average non-Hermiticity $\tau_\pm$ is very important, as it can determine whether we can obtain the real spectra in a non-Hermitian PC (see Supplementary Note 4). To see this, we set the average non-Hermiticity $\tau_\pm = 0$; then, the Hamiltonian (4) becomes

$$H = \frac{1}{\beta}\begin{pmatrix} W_-^{(0)} & -i\gamma\kappa W_+^{(0)} \\ -i\gamma\kappa^* W_-^{(0)} & W_+^{(0)} \end{pmatrix}, \tag{7}$$

where $\beta = 1 + \gamma^2|\kappa|^2$ is a real number.

Near the Γ point, we can expand the eigenfrequencies of the two linear bands for a small $k \equiv |\mathbf{k}|$ into

$$W_\pm^{(0)} = (\omega_d / c \pm v_g k / c)^2 \approx W_d \pm C_g k, \tag{8}$$

where $C_g = 2\omega_d v_g/c^2$, $W_d = (\omega_d/c)^2$, and ω_d is the Dirac-like point frequency. The band slope v_g can be obtained from numerical results in Figure 1A, where we assume v_g is a constant along all directions in the wave vector space, which is an excellent approximation of a conical dispersion at $k = 0$ for a system with C_{4v} symmetry [29]. The corresponding eigenvalues are

$$W_\pm = \frac{1}{\beta}\left(W_d \pm \sqrt{(C_g k)^2(1 + \gamma^2|\kappa|^2) - \gamma^2|\kappa|^2 W_d^2}\right). \tag{9}$$

EPs appear when the value under the square root is zero and form a ring in the wave vector space with a radius $k_c = k_b(1 + |\gamma\kappa|^{-2})^{-\frac{1}{2}} \leq k_b$, where $k_b = \omega_d/2v_g$ is the upper bound of the ring's radius. This means that the radius of the EP ring in $\mathbf{k}$ space cannot exceed k_b for any value of γ. In general, $|\kappa|$ is a small number, and the radius of the ring can be reduced to $k_c \approx k_b|\gamma\kappa|$. The eigenvalues are real outside the ring ($k > k_c$) and form complex conjugate pairs inside the ring ($k < k_c$). Therefore, by setting the average non-Hermiticity $\tau_\pm = 0$, we can obtain a real spectrum in a certain region (Supplementary Figure S1b gives a schematic of the band dispersions).

Before proceeding to the next subsection, the Hamiltonian (7) deserves more comments. Using the linear operator

$$\eta = \begin{pmatrix} W_- & 0 \\ 0 & -W_+ \end{pmatrix}, \tag{10}$$

the Hamiltonian (7) satisfies

$$\eta H(\gamma)\eta^{-1} = H(\gamma)^{\dagger} = H(-\gamma), \tag{11}$$

Implying that the Hamiltonian is pseudo-Hermitian and the operator η transforms the system with non-Hermiticity γ into its complex conjugate-paired system $-\gamma$. Unlike the traditional PT-symmetric system, the loss-gain distribution of our PC system is not PT-symmetric in real space, $n(x) \neq n^{*}(-x)$.

3 Results

3.1 Realizing the pseudo-Hermitian condition using a Dirac-like cone

The previous section shows that, by setting the average non-Hermiticity $\tau_{\pm} = 0$, the non-Hermitian Hamiltonian will become pseudo-Hermitian, and we can obtain the real spectra. For a PT-symmetric PC, $\tau_{\pm} = 0$ is automatically satisfied as the distributions of loss and gain within the unit cell are equal (see Supplementary Note 2 for details) [30]. However, for a non-PT-symmetric PC, achieving $\tau_{\pm} = 0$ is not an easy task. Now, we will show that, for a PC exhibiting a Dirac-like cone in the Brillouin zone center, we can always achieve the pseudo-Hermitian condition $\tau_{\pm} = 0$.

The eigenmode $u^{(0)}_{\mathbf{k}\pm}(\mathbf{r})$ in the quantity $F_{\Omega,mm'}$ depends on the structural details (such as the filling ratio r_c and the contrast between ε_A and ε_B) of the PC and can be computed numerically using COMSOL. Substituting the orthonormal relationship Equation (3) into the pseudo-Hermitian criteria $\tau_{\pm} = 0$, we solve a specific value of the loss-gain ratio ℓ_r

$$\ell_r = \frac{-F_{A,mm}}{F_{B,mm}} = \frac{-F_{A,mm}\varepsilon_B}{1 - F_{A,mm}\varepsilon_A}, \tag{12}$$

for both $m = +$ and $m = -$. Equation (12) shows that, to determine the value of ℓ_r, we must tune the system parameters so that the system satisfies $F_{\Omega,++} = F_{\Omega,--}$.

The band dispersions near the Dirac-like cone are shown in Figure 1A, and the quantities $\varepsilon_{\Omega}F_{\Omega,mm}$ of the three bands are plotted in Figure 1B. We can see that there is an intersection ($F_{\Omega,++} = F_{\Omega,--}$) at $k_x a/2\pi = 0.019$ (marked by the dashed line), and then Equation (12) can be used to determine the gain-to-loss ratio, which is found to be $\ell_r = -0.15235$. Physically, the existence of such an intersection is guaranteed by the band inversion in the Dirac-like cone [25]. The condition $F_{\Omega,++} = F_{\Omega,--}$ can always be achieved near the Dirac-like cone (see Supplementary Note 6 and Supplementary Figure S1 for details); therefore, $\tau_{\pm} = 0$ is realized at $k_x a/2\pi = 0.019$ as shown in Figure 1C. Note that the quantity $F_{\Omega,mm}$ should be a function of $\mathbf{k}$, but near the Dirac-like cone (except the Γ point), this quantity is almost a constant (as shown in Figure 1B), as the eigenmodes of the same point group are almost unchanged when the change of $\mathbf{k}$ is small. We can therefore assume that the values τ_m, and κ are independent of $\mathbf{k}$ in the considered Brillouin zone region. As shown in Figure 1C, by tuning $\ell_r = -0.15235$, we can obtain $\tau_{\pm} \approx 0$ near the Dirac-like cone (except very close to the Γ point, where $\tau_{-} \approx -\tau_{+}$). We can demonstrate that the pseudo-Hermitian condition at the Γ point is $\tau_{-} = -\tau_{+}$, which is less demanding than other points, as the symmetry at the Γ point is higher than that at other $\mathbf{k}$ points (see Supplementary Note 5 for details). Therefore, the pseudo-Hermitian criterion is approximately fulfilled for all the $\mathbf{k}$ points near the Dirac-like cone.

Now, we can calculate the band structures of a PC with loss-gain ratio $\ell_r = -0.15235$ to verify the validity of the pseudo-Hermitian Hamiltonian shown in Equation (7). We choose a non-Hermitian strength $\gamma = +0.367$ and plot the complex band structure along the $M - \Gamma - X$ direction in Figure 2A and B. The analytical results are shown by solid green lines, and the numerically results are calculated using COMSOL by open circles. The validity of our non-Hermitian Hamiltonian model is demonstrated by the good agreement between the two sets of results. We can see that EPs appear in both $\Gamma - X$ and $\Gamma - M$ directions. To show that these EPs form a ring in $\mathbf{k}$ space, we plot the three-dimensional complex band structure in Figure 2C and D using Equation (9) and COMSOL as shown by green surfaces (analytical results) and filled dots (numerical results), respectively. The analytical model (9) predicts that $k = k_c = 0.019(2\pi/a)$ form a ring of EPs, which is verified by COMSOL results. The eigenfrequencies inside the ring form complex-conjugate pairs, and outside the ring, we obtain the entirely real spectra.

However, entirely real spectra do not mean loss-gain compensation. To see this, we compare the system with non-Hermiticity $\gamma_{+} = +0.367$ with its complex conjugate-paired system $\gamma_{-} = -0.367$. If we replace γ_{+} by γ_{-}, the eigenfrequencies described by Equation (9) are the same, but the Hamiltonians (7) are different as described by Equation (11). In other words, these two systems (γ_{+} and γ_{-}) possess the same band dispersion, but the eigenfunctions are different (see Supplementary Note 7 for details); hence, they can display different scattering behaviors, as we will show later.

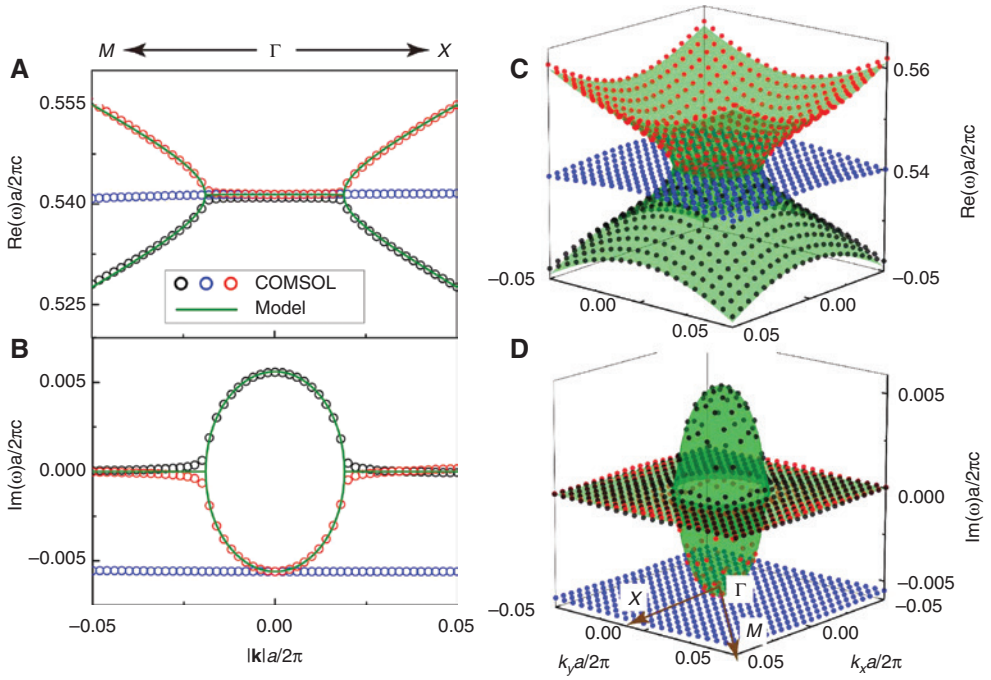

Figure 2: Band dispersions of pseudo-Hermitian bands.
The real parts (A and C) and the imaginary parts (B and D) of the complex eigenfrequencies along the $M-\Gamma-X$ direction and in the 2D Bloch k space. Open circles and solid dots are calculated using COMSOL, whereas green solid lines and green surfaces are calculated using the analytical model ($v_g = 0.295c$ and $|\kappa|^2 = 0.00318$). The bands outside the ring are entirely real. The parameters of 2D PC are $r_c = 0.1999a$, $\varepsilon_A = 12.5 + i\gamma$, $\varepsilon_B = 1 + i\gamma\ell_r$, $\gamma = +0.367$, and $\ell_r = -0.15235$.

3.2 Real spectra and CCM

The optical properties of an Hermitian PC carrying a Dirac-like cone in the Brillouin zone center can be described using an effective refractive index medium in which the effective permittivity and permeability are simultaneously zero at the Dirac-like point frequency. We have shown in the previous subsection that, by setting the average non-Hermiticity as zero, the spectra are real outside the ring of the EPs. It is interesting to see what type of EM corresponds to the non-PT-symmetric PC with real spectra. In this section, we will establish the EMT of non-Hermitian PC for describing the physics near the Γ point and study the related scattering properties.

We calculate the effective parameters using a boundary field averaging method [31]. Assuming that the wave $k = k\hat{x}$ propagates along the x direction, we define $Z = E_z/H_y = -\omega\mu/k = -k/(\omega\varepsilon)$ for a plane wave traveling in a homogeneous medium to express the ratio between the electric fields and the magnetic fields. For the inhomogeneous PC system, the average field ratio is defined as

$$Z^{\mathrm{PC}} = \frac{\int_{\mathrm{I}} E_z^{\mathrm{PC}} dy}{\int_{\mathrm{I}} H_y^{\mathrm{PC}} dy}, \tag{13}$$

where E^{PC} and H^{PC} are obtained from the eigenfields at the incident boundary I (the boundary of the unit cell along y direction). When we calculate effective parameters of the non-Hermitian PC as functions of frequency, the frequencies should take real-valued numbers, as in actual experiments the incident light comes with a real frequency. Therefore, within the PC, the eigenfields E^{PC} and H^{PC} are obtained by solving the "complex-valued $\mathbf{k}(\omega)$ vs. real-valued ω" band structures [32]. In Figure 3A, we plot the "complex-valued $\mathbf{k}(\omega)$" band structure of the non-Hermitian 2D PC calculated using COMSOL. We note that the imaginary parts of the bands (red lines) are almost zero, and for real bands, the "complex-valued $\mathbf{k}(\omega)$" band structure should agree well with the "complex-valued $\omega(\mathbf{k})$ vs. real-valued $\mathbf{k}$" band structure (see Supplementary Figure S7 for details). In Figure 3B, we plot Z^{PC} defined in Equation (13) for the bands with positive (dashed lines) and negative (solid lines) wave vectors, respectively, in Figure 3A. The effective permittivity and permeability can be calculated as follows:

$$\varepsilon_{\mathrm{e}} = \frac{-k}{\omega\varepsilon_0 Z^{\mathrm{PC}}}, \quad \mu_{\mathrm{e}} = \frac{-k}{\mu_0\omega} Z^{\mathrm{PC}}. \tag{14}$$

We plot the real and imaginary parts of $\varepsilon_{\mathrm{e}}(\mu_{\mathrm{e}})$ by squares (stars) in Figure 3C and D, respectively. Note that the

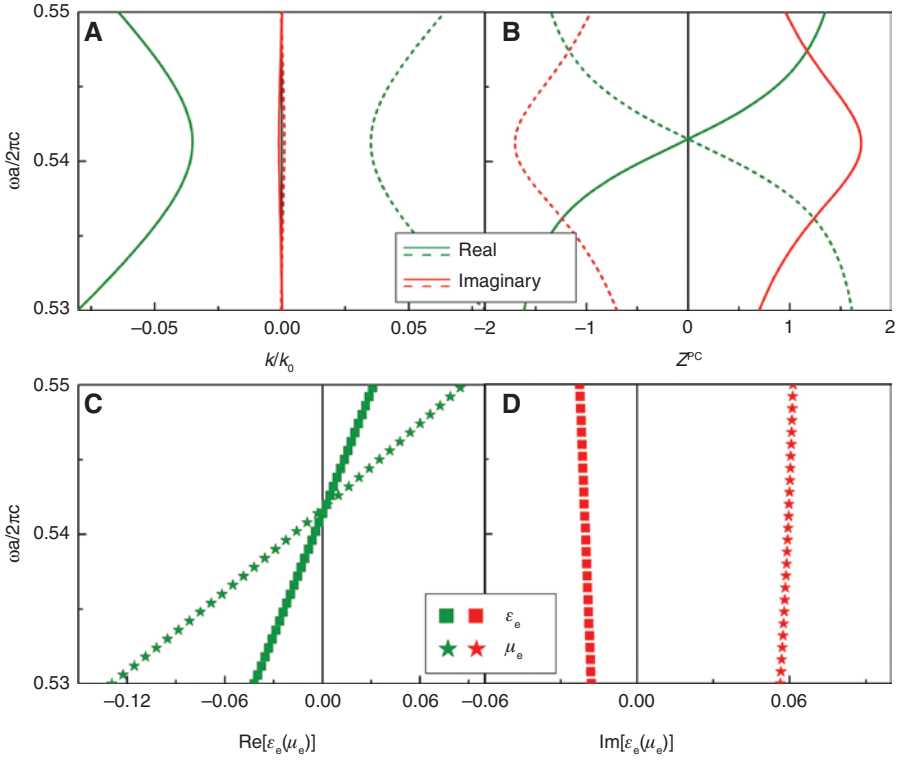

Figure 3: Effective parameters obtained from the real spectra as shown in Figure 2.
(A) Complex-valued $k(\omega)/k_0$ band and (B) averaged field ratio Z^{PC} calculated numerically from COMSOL. Bands with positive and negative wave vectors are represented by dashed and solid lines, respectively. The real (green) and imaginary (red) parts of the effective parameters ε_e and μ_e are plotted in squares and stars, respectively (C and D).

effective parameters obtained from the two bands (**k** and –**k**) are the same.

It is known that, for the Hermitian case, the effective parameters of the PC are real and approach zero near the Dirac-like point frequency, indicating that the PC can be treated as a zero refractive index medium [25]. When we introduce loss and gain into the PC, the effective parameters ε_e and μ_e obtain imaginary parts as shown in Figure 3D. However, we note that the effective refractive index $n_e^2=\varepsilon_e\mu_e=(k/k_0)^2$ is a real number, where k_0 is the wave vector in air. This automatically indicates that the inhomogeneous PCs behave like the homogeneous CCM whose refractive index is real but whose permittivity and permeability are complex numbers. The real effective refractive index does not necessarily imply a simple loss-gain compensation, as ε_e and μ_e have imaginary parts. Also, it can be proven that $\varepsilon_e^{(\gamma_+)}=\varepsilon_e^{(\gamma_-)^*}$ and $\mu_e^{(\gamma_+)}=\mu_e^{(\gamma_-)^*}$ (see Supplementary Note 8 for details).

The complex conjugate-paired systems (γ_+ and γ_-) have dramatically different effects on the scattering properties of electromagnetic waves. To demonstrate this, we consider a slab with thickness d formed by the homogeneous EM with the parameters ε_e and μ_e, as shown in Figure 4A. We assume that plane waves propagate along the x direction with an electric field polarized along the z direction and that the EM slab (blue region) is embedded in air (gray region). The electric field in the air can be written as $E(x)=a_1\exp(ik_0x)+b_1\exp(-ik_0x)$ for $x<-d/2$ and as $E(x)=b_2\exp(ik_0x)+a_2\exp(-ik_0x)$ for $x>d/2$. The amplitudes of incoming-propagating waves $(a_1, a_2)^T$ and outcoming-propagating waves $(b_2, b_1)^T$ are related by a scattering matrix [23].

$$S=\begin{pmatrix} t & r \\ r & t \end{pmatrix}=\frac{1}{M_{22}}\begin{pmatrix} 1 & M_{12} \\ M_{12} & 1 \end{pmatrix}, \tag{15}$$

where r and t represent the transmission and reflection coefficients of the slab for normal incident plane waves. The elements in S are

$$M_{12}=i\frac{n_e^2-\mu_e^2}{2n_e\mu_e}\sin(kd), \tag{16}$$

$$M_{22}=e^{(idk_0)}\left[\cos(kd)-i\frac{n_e^2+\mu_e^2}{2n_e\mu_e}\sin(kd)\right], \tag{17}$$

where $k=k_0n_e$ is the wave vector in the slab. The corresponding eigenvalues of the S matrix are

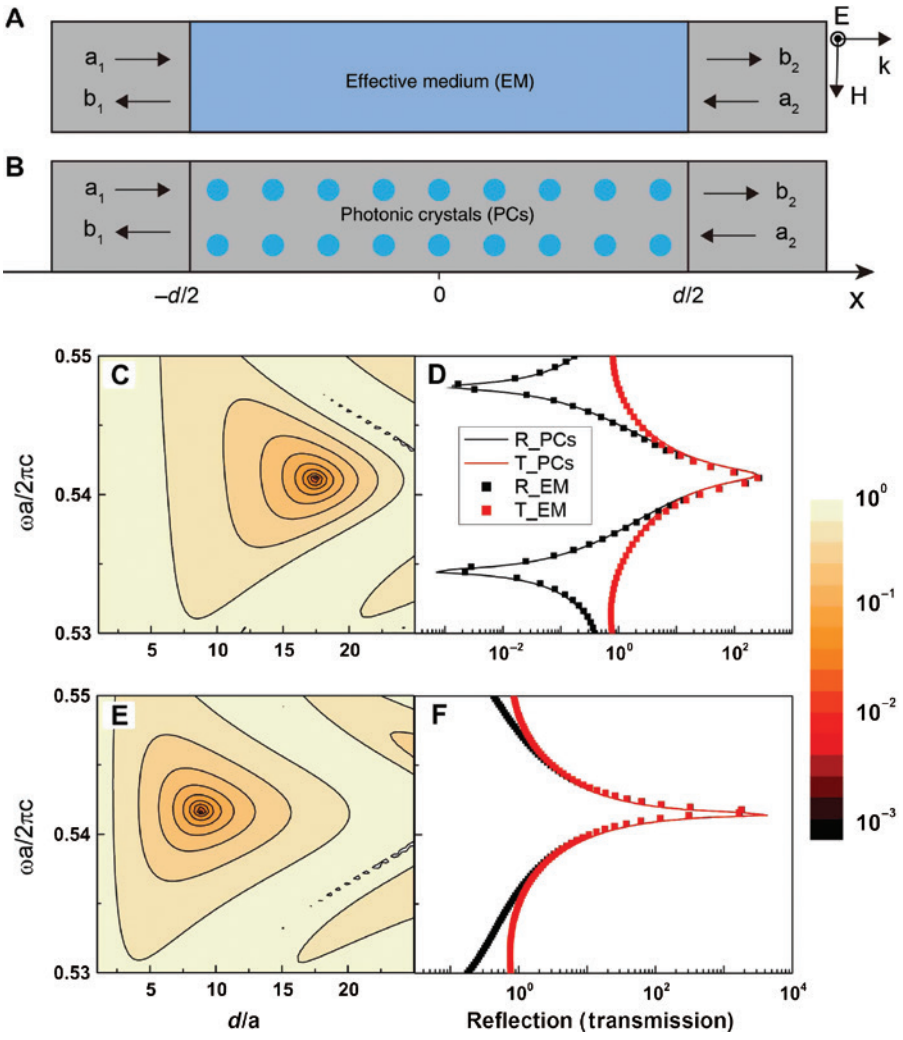

Figure 4: Scattering properties of CCM with effective parameters as shown in Figure 3.
Schematics of wave scattering in (A) EM slab and (B) PC slab. The contour plot of the value $1/\mathrm{Max}|\lambda_{\pm}|$ in the (ω, d) plane for EM slab with parameters (C) $\varepsilon_e^{(\gamma_+)}$, $\mu_e^{(\gamma_+)}$ and (E) $\varepsilon_e^{(\gamma_-)}$, $\mu_e^{(\gamma_-)}$. Black and red solid lines represent the reflection R and transmission T for PC slab and black and red squares represent EM slab, respectively. The non-Hermiticity strength of PCs is (D) $\gamma_+ = +0.367$ and (F) $\gamma_- = -0.367$. Slab thicknesses are $d/a = 17$ in (B) and $d/a = 9$ in (D).

$$\lambda_{\pm} = \frac{1}{M_{22}}[1 \pm M_{12}]. \tag{18}$$

These eigenvalues can be used to determine the S matrix poles ($1/\mathrm{Max}|\lambda_{\pm}| \to 0$) where lasing occurs. For a slab composed of CCM [$Im(n_e) = Im(k/k_0) = 0$], kd is a real number. For the S matrix to have poles, we require $M_{22} = 0$; therefore, we obtain

$$\frac{n_e^2 + \mu_e^2}{n_e \mu_e} = -2i\cot(kd). \tag{19}$$

To satisfy Equation (19), μ_e must be an imaginary number. Figure 3C and D shows the effective parameters of PCs with non-Hermiticity $\gamma_+ = +0.367$. We find $\mathrm{Re}[\mu_e^{(\gamma_+)}] = 0$ at $\omega a/2\pi c = 0.5416$, and we can solve Equation (19) to obtain the slab thickness $d/a = 17.4$. For PCs with non-Hermiticity $\gamma_- = -0.367$, the effective parameters are $\varepsilon_e^{(\gamma_+)} = \varepsilon_e^{(\gamma_-)*}$ and $\mu_e^{(\gamma_+)} = \mu_e^{(\gamma_-)*}$, and we can solve the slab thickness $d/a = 8.9$.

Figure 4C and E shows the contour plots of $1/\mathrm{Max}|\lambda_{\pm}|$ in the ($\omega a/2\pi c$, d/a) plane for EM slab with ($\varepsilon_e^{(\gamma_+)}$, $\mu_e^{(\gamma_+)}$) and ($\varepsilon_e^{(\gamma_-)}$, $\mu_e^{(\gamma_-)}$) respectively. To verify the scattering poles ($1/\mathrm{Max}|\lambda_{\pm}| \to 0$), in Figure 4B, we plot the transmission $T = |t|^2$ and reflection $R = |r|^2$ of slabs formed by homogeneous EM by squares and PCs by solid lines. The schematic of the one-dimensional scattering problem of slab formed by PCs is plotted in Figure 4B. We set the thickness of the slab $d/a = 17$, as the thickness of the slab formed by

PCs must be an integer. The good agreement between the EM and PCs results shows that the effective parameters shown in Figure 3C and D essentially reproduce the physics. We can see that the system indeed has the transmission and reflection singularities at $\omega a/2\pi c = 0.5416$ in Figure 4D. This indicates that we can observe the poles of the S matrix from the transport configuration. Similarly, the pole in Figure 4E at $d/a = 8.9$ and $\omega a/2\pi c = 0.5416$ for $(\varepsilon_e^{(\gamma_-)}, \mu_e^{(\gamma_-)})$ is also verified by the transmission and reflection singularities in Figure 4F, where $d/a = 9$. When we change the sign of γ, the real bands of the PCs remain almost the same, but the non-Hermitian PCs do not have time reversal symmetry. Although the refractive index satisfies $n_e^{(\gamma_+)} \approx n_e^{(\gamma_-)}$, the scattering phenomena change drastically as the effective permeability (or impedance) has imaginary parts, and $\mu_e^{(\gamma_+)} \neq \mu_e^{(\gamma_-)}$. This illustrates that the S matrix poles depend not only on the refractive index but also on the permeability as shown in Equation (19). The sum of the transmission and reflection is not equal to unity, although the effective refractive index of the slab is real. A real refractive index does not necessarily imply energy compensation. The focusing effect of our PCs as a lens is also different for these complex paired systems (see Supplementary Note 9 for details).

4 Discussion

In this work, we find that a non-PT-symmetric PC can have real spectra when the average non-Hermiticity within the unit cell is zero. We showed that the pseudo-Hermitian condition ($\tau_\pm = 0$) can always be fulfilled in two-component PCs carrying Dirac-like cones with bands arising from monopolar and dipolar resonances. These non-Hermitian PCs carrying Dirac-like cones can be used to realize CCM near the Dirac-like point frequency, where a real spectrum guarantees a real refractive index and the non-Hermiticity guarantees complex permittivity and permeability.

Acknowledgments: This work was supported by the Research Grants Council, University Grants Committee, Hong Kong (grant nos. AoE/P-02/12, N_HKUST608/17, 16303119, and C6013-18G, Funder Id: http://dx.doi.org/10.13039/501100002920) and the National Natural Science Foundation of China (grant nos. 11761161002, 61775243, Funder Id: http://dx.doi.org/10.13039/501100001809). K.D. acknowledges the funding from the Gordon and Betty Moore Foundation. We would like to thank Prof. Zhao Qing Zhang and Dr. Ruoyang Zhang for helpful discussions.

References

[1] Bender CM, Boettcher S. Real spectra in non-Hermitian Hamiltonians having PT symmetry. Phys Rev Lett 1998;80:5243–6.
[2] Bender CM, Brody DC, Jones HF. Complex extension of quantum mechanics. Phys Rev Lett 2002;89:270401.
[3] Mostafazadeh A. Exact PT-symmetry is equivalent to Hermiticity. J Phys A Math Gen 2003;36:7081–91.
[4] Bender CM. Making sense of non-Hermitian Hamiltonians. Rep Prog Phys 2007;70:947–1018.
[5] Rotter I. A non-Hermitian Hamilton operator and the physics of open quantum systems. J Phys A Math Theor 2009;42:153001.
[6] Mostafazadeh A. Pseudo-Hermitian representation of quantum mechanics. Int J Geomet Methods Mod Phys 2010;7:1191–306.
[7] Moiseyev N. Non-Hermitian quantum mechanics. Cambridge, New York: Cambridge University Press, 2011.
[8] Makris KG, El-Ganainy R, Christodoulides DN, Musslimani ZH. Beam dynamics in PT-symmetric optical lattices. Phys Rev Lett 2008;100:103904.
[9] Rüter CE, Makris KG, El-Ganainy R, Christodoulides DN, Segev M, Kip D. Observation of parity-time symmetry in optics. Nat Phys 2010;6:192–5.
[10] Regensburger A, Bersch C, Miri M-A, Onishchukov G, Christodoulides DN, Peschel U. Parity-time synthetic photonic lattices. Nature 2012;488:167–71.
[11] Heiss WD. The physics of exceptional points. J Phys A Math Theor 2012;45:444016.
[12] Ding K, Ma G, Xiao M, Zhang ZQ, Chan CT. Emergence, coalescence, and topological properties of multiple exceptional points and their experimental realization. Phys Rev X 2016;6:021007.
[13] Mostafazadeh A. Pseudo-Hermiticity versus PT symmetry: the necessary condition for the reality of the spectrum of a non-Hermitian Hamiltonian. J Math Phys 2002;43:205–14.
[14] Cannata F, Junker G, Trost J. Schrodinger operators with complex potential but real spectrum. Phys Lett A 1998;246:219–26.
[15] Tsoy EN, Allayarov IM, Abdullaev FK. Stable localized modes in asymmetric waveguides with gain and loss. Opt Lett 2014;39:4215–8.
[16] Makris KG, Musslimani ZH, Christodoulides DN, Rotter S. Constant-intensity waves and their modulation instability in non-Hermitian potentials. Nat Commun 2015;6:7257.
[17] Nixon S, Yang J. All-real spectra in optical systems with arbitrary gain-and-loss distributions. Phys Rev A 2016;93:031802.
[18] Hang C, Gabadadze G, Huang G. Realization of non-PT-symmetric optical potentials with all-real spectra in a coherent atomic system. Phys Rev A 2017;95:023833.
[19] Choy TC. Effective medium theory: principles and applications. Oxford, UK, Oxford University Press, 2015.
[20] Dragoman D. Complex conjugate media: alternative configurations for miniaturized lasers. Opt Commun 2011;284:2095–8.
[21] Imran A, Illahi A. On the effects of complex conjugate medium on TM scattering by a strip. J Electromagn Anal Appl 2011;3:267–70.
[22] Basiri A, Vitebskiy I, Kottos T. Light scattering in pseudopassive media with uniformly balanced gain and loss. Phys Rev A 2015;91:063843.
[23] Bai P, Ding K, Wang G. Simultaneous realization of a coherent perfect absorber and laser by zero-index media with both gain and loss. Phys Rev A 2016;94:063841.

[24] Xu Y, Fu Y, Chen H. Electromagnetic wave propagations in conjugate metamaterials. Opt Express 2017;25:4952.
[25] Huang X, Lai Y, Hang ZH, Zheng H, Chan CT. Dirac cones induced by accidental degeneracy in photonic crystals and zero-refractive-index materials. Nat Mater 2011;10:582–6.
[26] Zhen B, Hsu CW, Igarashi Y. Spawning rings of exceptional points out of Dirac cones. Nature 2015;525:354–8.
[27] Sakoda K. Optical properties of photonic crystals. In: Number 80 in Springer Series in Optical Sciences, 2nd ed. Berlin: Springer, 2005.
[28] Ding K, Zhang ZQ, Chan CT. Coalescence of exceptional points and phase diagrams for one-dimensional PT-symmetric photonic crystals. Phys Rev B 2015;92:235310.
[29] Sakoda K. Proof of the universality of mode symmetries in creating photonic Dirac cones. Opt Express 2012;20:25181.
[30] Szameit A, Rechtsman MC, Bahat-Treidel O, Segev M. PT-symmetry in honeycomb photonic lattices. Phys Rev A 2011;84:021806.
[31] Andryieuski A, Ha S, Sukhorukov AA, Kivshar YS, Lavrinenko AV. Bloch-mode analysis for retrieving effective parameters of metamaterials. Phys Rev B 2012;86:035127.
[32] Davanco M, Urzhumov Y, Shvets G. The complex Bloch bands of a 2D plasmonic crystal displaying isotropic negative refraction. Opt Express 2007;15:9681.

Supplementary Material: The online version of this article offers supplementary material (https://doi.org/10.1515/nanoph-2019-0389).